

# Journal of Biomedical Optics

BiomedicalOptics.SPIEDigitalLibrary.org

## High-speed phase-shifting common-path quantitative phase imaging with a piezoelectric actuator

Séverine Coquoz  
Amir Nahas  
Miguel Sison  
Antonio Lopez  
Theo Lasser

**SPIE.**

Séverine Coquoz, Amir Nahas, Miguel Sison, Antonio Lopez, Theo Lasser, "High-speed phase-shifting common-path quantitative phase imaging with a piezoelectric actuator," *J. Biomed. Opt.* **21**(12), 126019 (2016), doi: 10.1117/1.JBO.21.12.126019.

# High-speed phase-shifting common-path quantitative phase imaging with a piezoelectric actuator

Séverine Coquoz,<sup>†</sup> Amir Nahas,<sup>†</sup> Miguel Sison, Antonio Lopez, and Theo Lasser\*

Laboratoire d'Optique Biomédicale, École Polytechnique Fédérale de Lausanne, Station 17, 1015 Lausanne, Switzerland

**Abstract.** We present a phase-shifting quantitative phase imaging technique providing high temporal and spatial phase stability and high acquisition speed. A piezoelectric microfabricated phase modulator allows tunable modulation frequencies up to the kHz range. After assessing the quantitative phase accuracy with technical samples, we demonstrate the high acquisition rate while monitoring cellular processes at temporal scales ranging from milliseconds to hours. © The Authors. Published by SPIE under a Creative Commons Attribution 3.0 Unported License. Distribution or reproduction of this work in whole or in part requires full attribution of the original publication, including its DOI. [DOI: [10.1117/1.JBO.21.12.126019](https://doi.org/10.1117/1.JBO.21.12.126019)]

Keywords: quantitative phase imaging; common-path; high speed; cellular processes.

Paper 160721R received Oct. 18, 2016; accepted for publication Dec. 5, 2016; published online Dec. 23, 2016.

## 1 Introduction

Quantitative imaging of fast cellular processes is of high importance in life sciences. Classical phase imaging such as darkfield, Zernike phase contrast, or differential interference contrast provided new insight into these dynamic processes. However, these methods originally conceived for contrast enhancement did not provide quantitative phase information.

Over the past two decades, novel methods yielding quantitative phase information have been introduced such as digital holographic microscopy,<sup>1</sup> diffraction phase microscopy,<sup>2,3</sup> spatial light interference microscopy (SLIM),<sup>4</sup> quadriwave lateral shearing interferometry,<sup>5</sup>  $\tau$  interferometry,<sup>6,7</sup> partitioned aperture wavefront,<sup>8</sup> Fourier ptychographic microscopy,<sup>9,10</sup> transport-of-intensity equation-based techniques,<sup>11,12</sup> etc. Today, quantitative phase imaging (QPI) allows measuring optical path differences in the subnanometer range and has many technical applications demanding high accuracy. In biology and life sciences, QPI enables the measurement of the dry mass of a specimen and the quantitative monitoring of cell growth and cell proliferation.<sup>13</sup>

Many concepts for extracting the phase information are known in literature.<sup>14,15</sup> In phase-shifting interferometry, the phase difference between two interfering fields is varied. Off-axis interferometric techniques spatially modulate the phase by angularly shifting the two fields. Phase-shifting methods offer diffraction-limited resolution, while off-axis interferometric techniques have the advantage of being single-shot. Moreover, white-light illumination and common-path configuration are particularly interesting for biological studies as they offer high spatial phase sensitivity and high temporal stability.<sup>15</sup> Lastly, setups that can be attached to standard bright-field microscopes without modification of the illumination source are convenient and may ease the use of QPI in biology or clinical diagnosis.

Recently, interferometric techniques offering several benefits have been proposed including portable, common-path, white-

light, phase shifting approaches such as SLIM,<sup>4</sup> Fourier phase microscopy (FPM),<sup>16,17</sup> and white-light QPI unit.<sup>18</sup> These techniques provide high resolution, high stability, and speckle-free phase images. However, phase shifting is performed based on liquid-crystal devices having low switching rates, which limits the acquisition speed of these techniques.

In this paper, we propose a new phase-shifting QPI method overcoming this speed limitation while offering the benefits of white-light illumination and common-path geometry. Our approach, termed piezo-based Fourier phase microscopy (pFPM), can also be implemented as a simple add-on module to a conventional microscope. Fast phase modulation with minimal effects of dispersion or polarization can be achieved with a customized piezo-driven microfabricated mirror module. Our mirror design allows phase shifting rates up to several kilohertz. In consequence, our technique is only limited by the camera frame rate. These features pave the way to many applications demanding high acquisition rates such as imaging of fast dynamic cellular processes.

## 2 Materials and Methods

### 2.1 pFPM Setup

We start with a description of the setup, which is depicted in Fig. 1. As in SLIM<sup>4</sup> or FPM,<sup>16,17</sup> our pFPM module can be attached to a commercial or custom-made phase contrast microscope. The sample is illuminated by a white light source (halogen lamp, Osram). A condenser annulus (Ph3 ring, Axiovert 100, Zeiss) produces a ring illumination to spatially separate the scattered and unscattered light in the back focal plane of the objective. This plane is relayed by a first Fourier lens  $L_1$  ( $f_1 = 200$  mm, Thorlabs) onto a piezo-based phase shifting module as described below. The image is finally acquired by the camera (MV1-D1024E-160-CL, Photonfocus,  $1024 \times 1024$  pixels, 150 fps) via a second Fourier lens  $L_2$  ( $f_2 = 200$  mm, Thorlabs). The microscope was equipped with a  $100 \times 1.45$  NA oil-immersion objective (Zeiss, effective NA = 0.6). The field of view (FOV) obtained with this configuration was  $120 \times 120 \mu\text{m}^2$ .

\*Address all correspondence to: Theo Lasser, E-mail: [theo.lasser@epfl.ch](mailto:theo.lasser@epfl.ch)

<sup>†</sup>These authors contributed equally to this work.

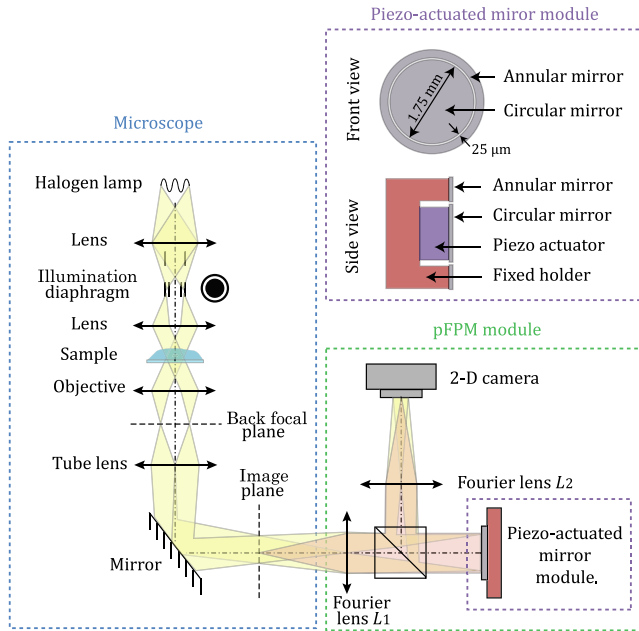


**Fig. 1** Schematic of the pFPM setup.  $L_1$  relays the back focal plane of the objective onto a piezo-based mirror module.  $L_2$  reconstructs the final image at the camera plane, which is conjugated to the microscope's image plane. The mirror module is composed of a fixed annular mirror and a piezo-actuated circular inner mirror.

## 2.2 Phase-Shifting Piezo-Actuated Module

The phase shifting module consists of a piezo-actuated circular inner mirror and a fixed annular outer mirror. The module is based on silicon technology taking full advantage of the high surface quality and flatness. The mirror pair was fabricated using photolithography and dry etching processing on a standard wafer ( $\langle 100 \rangle$ , 100-mm diameter, 525- $\mu\text{m}$  thick). To improve the reflective properties of the surface, a 200-nm layer of aluminum was added by plasma-enhanced chemical vapor deposition on top of a 10-nm layer of chromium. These mirrors were characterized with an optical profiling system (Wyko NT1100, Veeco) giving a root mean square roughness  $R_{\text{RMS}}$  of 2.03 nm ( $\sim \lambda/200$ ) and a peak-to-valley smaller than 15 nm ( $\sim \lambda/40$ ). The inner diameter of the annular mirror was determined by matching the dimensions of the image of the ring illumination and was found to be 1.8 mm. The circular mirror has a diameter of 1.75 mm, resulting in a 25  $\mu\text{m}$  inter-mirror gap minimizing the losses while preventing any friction. The inner mirror was mounted on a piezoelectric actuator (PE4, Thorlabs) and inserted on a three-axis translation stage in the center of the annular mirror.

The circular mirror reflects the inner part of the scattered light from the sample while the annular one reflects the unscattered field and, therefore, plays the role of reference. The piezoelectric actuator translates the inner mirror with respect to the outer one and thus, modulates the phase delay between the scattered and unscattered light. By calibrating the mirror displacements to steps corresponding to the increments of  $\pi/2$  using a Michelson interferometer, the four phase shifts required for QPI can be accessed. Our design results in a moving mirror of small size and small mass ( $m = 5.3$  mg), thus allowing for a very fast tunable modulation rate up to several kilohertz. The same mirror pair can be used with different microscope objectives by adding an appropriate relay system.

## 2.3 Phase Retrieval

The QPI can be retrieved as follows.<sup>4,16</sup> Let  $U_r$  and  $U_s$  be the reference and scattered light field amplitudes, and  $\Delta\varphi$  is the phase difference between them. At each phase step  $m$ , the intensity in the image plane at each pixel of the camera is given by

$$I_m(\Delta\varphi) = |U_r|^2 + |U_s|^2 + 2 \cdot U_r \cdot U_s \cdot \tilde{S}(\Delta\varphi + m\pi/2) \cdot \cos(\Delta\varphi + m\pi/2). \quad (1)$$

Here,  $\tilde{S}$  represents the normalized illumination power spectrum. The phase difference  $\arg(U_s, U_r)$  can be determined (see Chapter 6 in Ref. 14) as

$$\Delta\varphi = \tan^{-1} \left( \frac{I_4 - I_2}{I_1 - I_3} \right). \quad (2)$$

The phase associated with the image field can be retrieved as  $\arg(U_s + U_r, U_r)$ :

$$\varphi = \tan^{-1} \left[ \frac{\beta \sin(\Delta\varphi)}{1 + \beta \cos(\Delta\varphi)} \right], \quad (3)$$

where  $\beta = \alpha U_s / U_r$ . The factor  $\alpha$  is a system calibration constant experimentally determined on a technical sample.

In this work, we use discrete  $0, \pi/2, \pi$ , and  $3\pi/2$  phase steps and calculate the phase images from the recorded phase-shifted data using an interlaced scheme similar to a running average. In other words, a new phase image is calculated after each acquisition of a new phase-shifted frame. Note that this interlaced processing induces correlations over four calculated phase images. In this manner, we achieve camera frame-rate limited phase acquisition speed. For higher frequency applications using a faster camera, an integrating bucket approach would be more appropriate.<sup>14,19</sup>

## 2.4 Cell Dry Mass Calculation

QPI methods can also be used for dry mass measurements.<sup>20–22</sup> The dry mass (i.e., the nonaqueous content) density  $\sigma$  of a cell is calculated as

$$\sigma(x, y) = \frac{\lambda}{2\pi\gamma} \Delta\varphi(x, y) \quad (4)$$

with  $\lambda$  the center wavelength and  $\gamma$  the average of reported values for the refractive increment of protein (0.2 mL/g).<sup>20</sup> The total dry mass for each cell is calculated by summing the dry mass density over the area of the cell. For the *Escherichia coli* growth measurement described below, image segmentation of each frame was performed by the open-source Schnitzcells software.<sup>23</sup>

## 3 Results

### 3.1 Validation of pFPM

The experimental results are summarized in Figs. 2–4. First, we validate the quantitative character of our approach on a technical sample composed of a drop of polystyrene microspheres with a diameter of 1  $\mu\text{m}$  and a refractive index of  $n_{\text{ps}} = 1.60$  at 550 nm (polysciences) between a glass coverslip and a 0.5% agarose gel ( $n_{\text{agarose}} = 1.33$  at 550 nm). Figures 2(a) and 2(b)

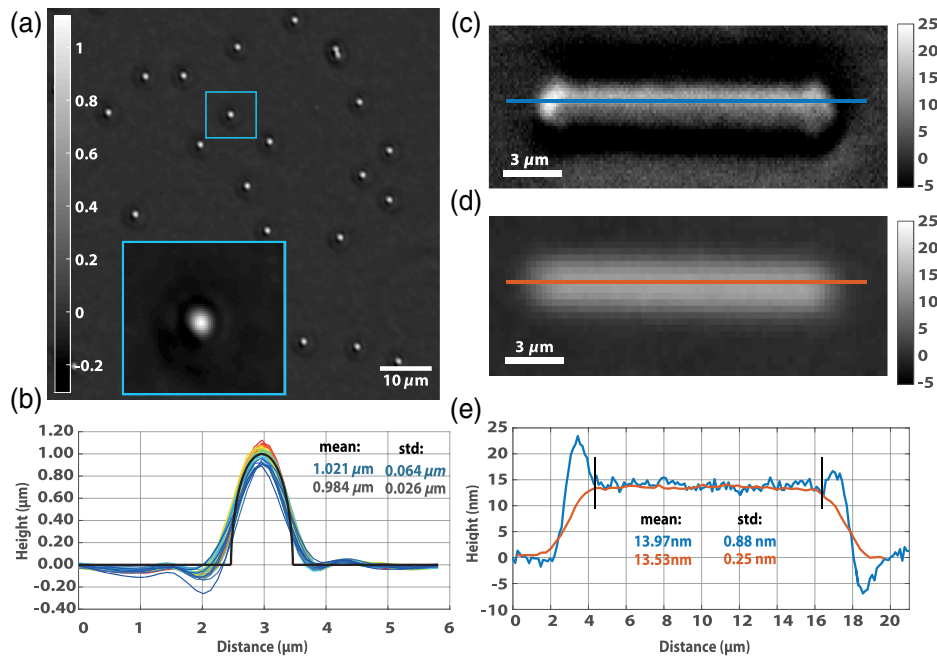


**Fig. 2** Quantitative assessment of pFPM demonstrated on two technical samples. (a) Height map with a zoom-in of one of the 1  $\mu\text{m}$  polystyrene beads. (b) Height profiles along 28 microspheres (color) and the ideal semicircle (black). The mean and STD measured with pFPM (blue) and specified by the supplier (gray) are indicated. (c) Height map of a technical sample (Lyncée Tec SA) obtained with pFPM. (d) Corresponding map measured with an optical profiling system. (e) Height profiles corresponding to the two lines in (c) and (d). The results for both samples are in good agreement with the specifications.

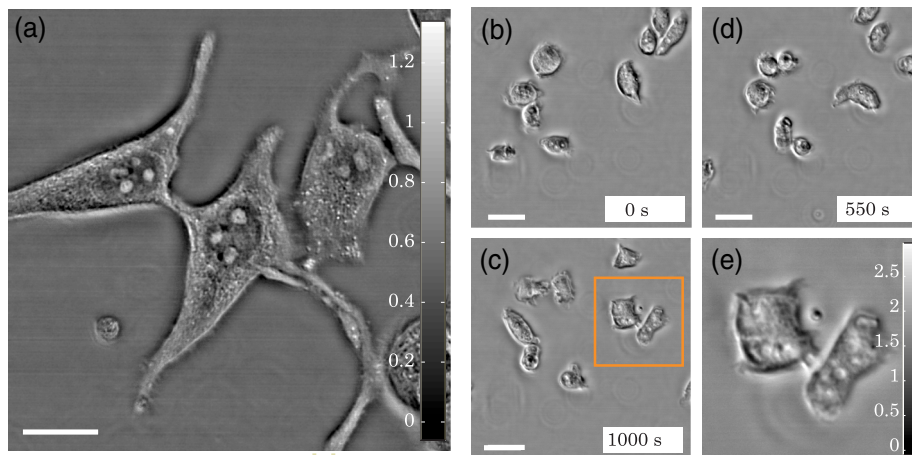


**Fig. 3** (a) One frame of a pFPM quantitative phase recording (Video 1) of live HeLa cells imaged at 150 Hz. Subcellular dynamics, e.g., motion of vesicles, is clearly visible. (b)–(d) Several frames from a 30-min acquisition (see Video 2) showing cell division (highlighted in cyan in Video 2), exocytosis of a 1  $\mu\text{m}$  bead (highlighted in blue), and vacuolar dynamics in *D. discoideum*. (e) Zoom of the area highlighted in (d). Scale bars: 20  $\mu\text{m}$ . Color bars: radians. (Video 1, QuickTime, 5.8 MB) [URL: <http://dx.doi.org/10.1117/1.JBO.21.12.126019.1>] and (Video 2, QuickTime, 17 MB) [URL: <http://dx.doi.org/10.1117/1.JBO.21.12.126019.2>].

show the obtained quantitative height image and horizontal profiles through the 28 beads in the FOV. The mean and standard deviation (STD) of the measured beads' heights are 1.021 and 0.064  $\mu\text{m}$ , which is in good agreement with the microspheres' specifications (mean = 0.984  $\mu\text{m}$ , STD = 0.026  $\mu\text{m}$ ). The non-spherical shape of the beads is due to the convolution with the point spread function (PSF) of our system. Small misalignments in the pFPM module create a small asymmetry of the PSF.

Next, we measured several test samples (Lyncée Tec SA) consisting of bars of several dimensions. The pFPM height image of a bar with 3- $\mu\text{m}$  width, 15- $\mu\text{m}$  length, and a specified 15-nm height is shown in Fig. 2(c). A height profile along the length of the bar is shown in Fig. 2(e). To validate the pFPM measurements, we imaged the same bar with an optical profiler (Wyko NT1100, Veeco). The results are shown in Figs. 2(d) and 2(e). The height measurements with both techniques are in

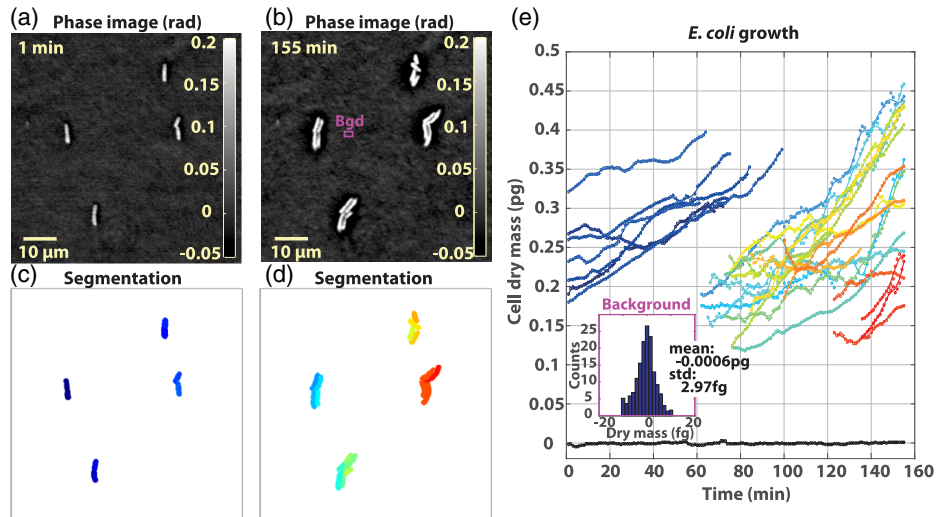


**Fig. 4** QPI measurement of *E. coli* growth with pFPM (Video 3). (a) and (b) QPIs at time  $t = 0$  h and 2 h 35, respectively. (c)–(d) Corresponding segmented images. (e) Dry mass versus time for the segmented cells in (c)–(d). Inset: histogram of the dry mass fluctuations associated with a background region having the same area as the average cell size and highlighted in (b) (Video 3, MPEG, 4.7 MB) [URL: <http://dx.doi.org/10.1117/1.JBO.21.12.126019.3>].

excellent agreement, with a mean height along the bar of 13.97 nm obtained with the pFPM and 13.53 nm obtained with the optical profiler. The means and STDs of the measured height with both techniques were calculated between the two vertical bars shown in Fig. 2(e).

Note that because of the spatial separation of the scattered and unscattered light in the Fourier plane, pFPM images show a “halo effect” and artifacts related to high-pass spatial filtering well-known in phase microscopy.<sup>24–26</sup> This halo effect is particularly visible on the second technical sample, both on the height map and the profile in Fig. 2(c).

### 3.2 Imaging of Fast Subcellular Dynamics in HeLa Cells

Now that the validity of the phase measurement with pFPM has been demonstrated, we show its high speed capability by capturing subcellular dynamics in live HeLa cells. HeLa cells were cultured at 37°C with 5% CO<sub>2</sub> using minimum essential medium (MEM) eagle with Earles salts, L-glutamine, sodium bicarbonate complemented with 10% fetal bovine serum, 1× penicillin–streptomycin, 1× GlutaMAX, 1× MEM nonessential amino acids solution (all products purchased from Thermo Fischer Scientific Inc.). Cells were plated in 35 mm Fluorodish Cell Culture Dishes (World Precision Instruments) and imaged in Hank’s balanced salt solution culture medium.

A snapshot of a dynamic pFPM image sequence acquired at 150 fps is shown in Fig. 3(a). Video 1 shows that subcellular features and dynamics, such as movements of cytoplasmic vesicles, are clearly observed.

### 3.3 Imaging of Division and Exocytosis in Dictyostelium discoideum

Our pFPM setup was also used to observe samples across longer time scales with subsecond acquisition speeds up to 150 Hz. Here, we used *D. discoideum* cells, a model organism uniquely suited for studying cytokinesis, cell motility, phagocytosis, chemotaxis, etc.<sup>27</sup> These amoeba were cultured at room

temperature in Petri dishes in HL5c culturing medium (Formedium). For imaging, 1 ml of cells in HL5c were transferred to glass-bottom dishes (MatTek Corporation) and allowed to attach for a few minutes before starting the acquisition.

Figures 3(b)–3(e) show a few frames from a time-lapse video of *D. discoideum* imaged during 30 min at a rate of one phase image per second. Endocytosis and exocytosis events were induced by adding 1-μm diameter microspheres to the cell sample. As can be seen in Video 2, the high resolution of our system allows visualizing and tracking subcellular structures such as vacuoles. Because the amoeba cannot digest the microspheres they engulf, they release them by exocytosis after some time. Such an event can be observed at  $t \approx 940$  s in the area outlined in green in Video 2. Note that the engulfed bead can easily be tracked over time inside the *D. discoideum*. In addition, a cell division (occurring around  $t = 500$  s) is also highlighted in the video.

### 3.4 Growth Measurement of E. coli Bacteria

Our instrument exhibits a high temporal stability enabling time-lapse experiments over durations of several hours or more. This is illustrated here on a dry mass measurement of *E. coli* bacteria growing at 37°C. *E. coli* K-12 MG1655 were cultured overnight at 37°C in Lysogeny Broth (LB) (Lennox) medium (Carl Roth). These cultures were then diluted 1000× in LB medium. After incubating for approximately 1 h, 3 μL of this subculture was pipetted on a glass-bottom dish (MatTek) and covered by a thin agar slab with minimal medium (1.5% agarose, M9 5×, and glucose) (Sigma-Aldrich). In order to prevent the agar slab from drying, 80 μL of water was added to the corners of the dish.

Figure 4 shows the results of this experiment. *E. coli* growth was recorded by acquiring one phase image every minute. Phase images (a–b), segmentation (c–d), and dry mass growth curves (e) for small colonies of bacteria originating from four initial single *E. coli* cells are presented in Fig. 4 and Video 3. The dry mass noise is characterized from a region without any cells [highlighted in Fig. 4(b)] and having the same area as the average cell size. Background variations are shown by the black curve and histogram in Fig. 4(e). We achieve a STD of the

dry mass of 2.97 fg, indicating that our pFPM system is stable enough to perform sensitive growth measurements. Note that this noise is not intrinsic to the system but partly results from the culture environment and would be different for other samples. Compared to the average cell dry mass (= 0.2655 pg), background fluctuations are negligible here. Variations of the calculated dry mass values mostly result from differences in the segmented areas from frame to frame.

## 4 Summary and Discussion

In summary, we introduced a high-speed phase-shifting QPI method only limited by the camera frame rate. This was achieved by using a phase modulator based on a piezo-driven microfabricated mirror module. We first demonstrated the validity of pFPM on technical samples. Biological processes were then imaged at different time scales on different cell samples.

Our method presents the virtues of common-path and white-light QPI methods, i.e., a high temporal stability and a high spatial sensitivity. Our module can also easily be attached to a classical microscope. In addition to these qualities, our system also exhibits camera frame-rate limited acquisition achieved by piezo-based phase shifting. Moreover, the piezoelectric actuator allows large travel ranges enabling potential applications such as spectroscopic imaging.

Based on our results, we anticipate that the proposed technique may allow applications in many biological fields such as fast subcellular dynamics, biomechanics, and elastography.

## Disclosures

The authors declare no competing interests.

## Acknowledgments

We are thankful to Professor Gabriel Popescu for the stimulating discussions during his summer stay at EPFL. We would like to thank Katrin Schneider and Matthieu Delincé (LMIC, EPFL, Switzerland) as well as Azat Sharipov (LOB, EPFL) for providing us with the biological samples. The test samples were kindly provided by Etienne Cuche of Lyncée Tec SA. We also thank Jérôme Extermann (LOB, EPFL) for reviewing the manuscript. Finally, we acknowledge the staff of the CMI of EPFL for help with the fabrication of the mirror module. This work was supported in part by the Swiss National Fonds (SNF Grant 205320L\_150191).

## References

1. M. K. Kim, "Principles and techniques of digital holographic microscopy," *SPIE Rev.* **1**(1), 018005 (2010).
2. G. Popescu et al., "Diffraction phase microscopy for quantifying cell structure and dynamics," *Opt. Lett.* **31**(6), 775–777 (2006).
3. B. Bhaduri et al., "Diffraction phase microscopy with white light," *Opt. Lett.* **37**, 1094–1096 (2012).
4. Z. Wang et al., "Spatial light interference microscopy (SLIM)," *Opt. Express* **19**, 1016–1026 (2011).
5. P. Bon et al., "Quadriwave lateral shearing interferometry for quantitative phase microscopy of living cells," *Opt. Express* **17**, 13080–13094 (2009).
6. N. Shaked, "Quantitative phase microscopy of biological samples using a portable interferometer," *Opt. Lett.* **37**(11), 2016–2018 (2012).
7. P. Girshovitz and N. T. Shaked, "Compact and portable low-coherence interferometer with off-axis geometry for quantitative phase microscopy and nanoscopy," *Opt. Express* **21**, 5701–5714 (2013).
8. A. B. Parthasarathy et al., "Quantitative phase imaging using a partitioned detection aperture," *Opt. Lett.* **37**, 4062–4064 (2012).

9. G. Zheng, R. Horstmeyer, and C. Yang, "Wide-field, high-resolution Fourier ptychographic microscopy," *Nat. Photonics* **7**(9), 739–745 (2013).
10. X. Ou et al., "Quantitative phase imaging via Fourier ptychographic microscopy," *Opt. Lett.* **38**(22), 4845–4848 (2013).
11. M. R. Teague, "Deterministic phase retrieval: a Green's function solution," *J. Opt. Soc. Am.* **73**(11), 1434 (1983).
12. A. Barty et al., "Quantitative optical phase microscopy," *Opt. Lett.* **23**(11), 817–819 (1998).
13. K. Lee et al., "Quantitative phase imaging techniques for the study of cell pathophysiology: from principles to applications," *Sensors* **13**(4), 4170–4191 (2013).
14. D. Malacara, M. Servín, and Z. Malacara, *Interferogram Analysis for Optical Testing*, 2nd ed., CRC Press, Boca Raton (2005).
15. G. Popescu, *Quantitative Phase Imaging of Cells and Tissues*, McGraw-Hill, New York (2011).
16. G. Popescu et al., "Fourier phase microscopy for investigation of biological structures and dynamics," *Opt. Lett.* **29**(21), 2503–2505 (2004).
17. B. Bhaduri, K. Tangella, and G. Popescu, "Fourier phase microscopy with white light," *Biomed. Opt. Express* **4**, 1434 (2013).
18. Y. Baek et al., "White-light quantitative phase imaging unit," *Opt. Express* **24**(9), 9308 (2016).
19. J. C. Wyant, "Use of an ac heterodyne lateral shear interferometer with real-time wavefront correction systems," *Appl. Opt.* **14**(11), 2622–2626 (1975).
20. R. Barer, "Interference microscopy and mass determination," *Nature* **169**, 366–367 (1952).
21. H. Davies and M. Wilkins, "Interference microscopy and mass determination," *Nature* **169**, 541–541 (1952).
22. G. Popescu et al., "Optical imaging of cell mass and growth dynamics," *Am. J. Physiol.* **295**, C538–C544 (2008).
23. J. W. Young et al., "Measuring single-cell gene expression dynamics in bacteria using fluorescence time-lapse microscopy," *Nat. Protocols* **7**, 80–88 (2012).
24. F. Zemike, "How I discovered phase contrast," *Science* **121**(3141), 345–349 (1955).
25. T. Wilson and C. J. R. Sheppard, "The halo effect of image processing by spatial frequency filtering," *Optik* **59**(1), 19–23 (1981).
26. T. H. Nguyen et al., "Quantitative phase imaging with partially coherent illumination," *Opt. Lett.* **39**(19), 5511–5514 (2014).
27. S. Bozzaro, "The model organism *Dictyostelium discoideum*," in *Dictyostelium Discoideum Protocols*, L. Eichinger and F. Rivero, Eds., pp. 17–37, Humana Press, New York (2013).

**Séverine Coquoz** completed her BS and MS degrees in microengineering at École Polytechnique Fédérale de Lausanne (EPFL). She is a PhD student in the Laboratoire d'Optique Biomédicale (LOB) at EPFL, Switzerland. Her thesis research is focused on developing coherent imaging techniques for the study of cellular dynamics.

**Amir Nahas** obtained his PhD at the Institut Langevin in Paris, France. He is a postdoctoral fellow in the LOB at EPFL. His research interests include phase imaging, OCM, and full-field OCT, with a focus on photothermal imaging and elastography.

**Miguel Sison** received his undergraduate studies degree in applied physics at the University of the Philippines and acquired his Master of Photonics degree at the Friedrich-Schiller-University Jena. He is a PhD student at the Doctoral School of Photonics of EPFL. His research interests include coherent microscopy, biomedical optics, and nanoparticles as specific labels for live-cell imaging.

**Antonio Lopez** obtained his engineering degree in microtechnology at the Engineering School of Yverdon, Switzerland. He currently works as a research engineer in the LOB at EPFL. He develops and microfabricates electronic and precision mechanical devices for optical instruments including super-resolution microscopes.

**Theo Lasser** is a full professor and head of the Laboratoire d'Optique Biomédicale in the Department of Microengineering of EPFL. He also has many years of experience in industry and more particularly in Carl Zeiss, where he served as head of R&D and general manager. His research is mainly focused on the development of optical functional imaging methods for applications in life sciences and medicine.